Article:
Gaulier, G., Dietschi, Q., Bhattacharyya, S. et al. (10 more authors) (2021) Ultrafast pulse shaping modulates perceived visual brightness in living animals. Science Advances, 7 (18). eabe1911. ISSN 2375-2548

https://doi.org/10.1126/sciadv.abe1911

APPLIED PHYSICS

Ultrafast pulse shaping modulates perceived visual brightness in living animals

Geoffrey Gaulier[1], Quentin Dietschi[2], Swarnendu Bhattacharyya[3], Cédric Schmidt[1†], Matteo Montagnese[1], Adrien Chauvet[1‡], Sylvain Hermelin[1§], Florence Chiodini[4], Luigi Bonacina[1], Pedro L. Herrera[5], Ursula Rothlisberger[3], Ivan Rodriguez[2], Jean-Pierre Wolf[1]*

Vision is usually assumed to be sensitive to the light intensity and spectrum but not to its spectral phase. However, experiments performed on retinal proteins in solution showed that the first step of vision consists in an ultrafast photoisomerization that can be coherently controlled by shaping the phase of femtosecond laser pulses, especially in the multiphoton interaction regime. The link between these experiments in solution and the biological process allowing vision was not demonstrated. Here, we measure the electric signals fired from the retina of living mice upon femtosecond multipulse and single-pulse light stimulation. Our results show that the electrophysiological signaling is sensitive to the manipulation of the light excitation on a femtosecond time scale. The mechanism relies on multiple interactions with the light pulses close to the conical intersection, like pump-dump (photoisomerization interruption) and pump-repump (reverse isomerization) processes. This interpretation is supported both experimentally and by dynamics simulations.

INTRODUCTION

Unlike the spatial phase of light, which contributes to the image formation on the retina, the spectral phase of light is assumed to play no role in vision. Pioneering experiments using femtosecond lasers showed that the primary process involved in the visual response relies on the ultrafast photoisomerization of the retinal moiety in membrane proteins, such as rhodopsin (*1*–*3*). In these spectroscopic studies of molecules in solution, the phase φ(ω) of each spectral component of the electric field was shown to play a crucial role, as it is directly transferred to resonant excited-states via the electric dipole Hamiltonian $H_1 = -\boldsymbol{d}\cdot\boldsymbol{E}(t)$, with $\boldsymbol{E}(t) = \frac{1}{2\pi}\int(\boldsymbol{A}(\omega)\, e^{-i\varphi(\omega)})\, e^{i\omega t}\, d\omega$. It was shown that the dynamics of the wave packet in the excited-state potential surface can be manipulated by both the amplitude $\boldsymbol{A}(\omega)$ and the phase φ(ω) of the laser electric field. In other words, the unitary evolution operator $U(t)$ of the molecule is now determined by $\frac{d}{dt}U(t) = -\frac{i}{\hbar}[H_0 - \boldsymbol{d}\cdot\boldsymbol{E}(t)]\,U(t)$ (*4*). A key point is that the experiments in solution showed that the retinal photoisomerization yield can be controlled by the spectral phase φ(ω) alone, without modifying the spectral amplitudes $\boldsymbol{A}(\omega)$ (*5*–*7*). The coherent control of the retinal isomerization in solution using excited-state dynamics was realized either intrapulse (*5*–*7*) or with multipulse sequences, like pump-probe or pump-dump schemes (*8*–*10*). One of the founding concepts of the coherent control paradigm, the celebrated "Tannor-Kosloff-Rice" scheme (*11*–*13*), consists in the use of a pump-dump strategy to control the molecular excited-state dynamics and induce a selective bond break in the ground state.

In the quest of demonstrating optical control on systems of increasing complexity, recently, Paul *et al.* demonstrated manipulation of neural signaling ex vivo in the brain of transgenic mice (using patch clamp techniques on the retinal tissue). The authors applied coherent control of optogenetic response acting upon the two-photon absorption of channelrhodopsin-2 (*14*). Here, we address the fundamental question: Can we modulate a natural function (i.e., the retinal response) in a wild-type living animal the same way we can control the isomerization of individual rhodopsin molecules? We show that this procedure is successful using phase-shaped ultrashort laser pulses at intensities in the multiphoton regime but systematically within eye physiological response. These conclusions contrast with what is usually assumed from the eye physiology and thus shed new light on our vision's capabilities (*15*–*17*).

RESULTS AND DISCUSSION

In a first approach, the modulation of the ultrafast response of the retina is achieved following a multipulse approach. To this end (Fig. 1), we illuminated the right eye of a living mouse (C57BL/6 strain) with two laser pulses, one centered at 535 nm [30 nm full width at half maximum (FWHM)] and the other at 800 nm (30 nm). The temporal order and the separation between the two colors could be freely chosen from −250 to +250 fs (negative values refer to 800 nm preceding 535 nm). The electrical activity of the retina upon laser illumination was recorded on the eye by the measurement of evoked potentials (*18*) with a high-sensitivity electroretinograph (ERG) (see Materials and Methods). The ERG signals were captured by electrodes in contact with each eye, the left eye providing a reference. Sequences of five pulses at the 1-kHz laser repetition rate were used to illuminate

[1]Group of Applied Physics, University of Geneva, 22 Ch. de Pinchat, 1211 Geneva, Switzerland. [2]Department of Genetics and Evolution, University of Geneva, 30 Quai Ansermet, 1211 Geneva, Switzerland. [3]Institute of Chemical Sciences and Engineering, Ecole Polytechnique Fédérale de Lausanne, 1015 Lausanne, Switzerland. [4]Biobanque de tissus thérapeutiques, Department of Diagnostic, University Hospitals of Geneva, Rue Gabrielle-Perret-Gentil 4, 1205 Geneva, Switzerland. [5]Department of Genetic Medicine and Development, University of Geneva, 1 Rue Michel-Servet, 1211 Geneva, Switzerland.
*Corresponding author. Email: jean-pierre.wolf@unige.ch
†Present address: Haute école du paysage, d'ingénierie et d'architecture (HEPIA), Rue de la Prairie 4, 1202 Geneva, Switzerland.
‡Present address: Department of Chemistry, Dainton Building, University of Sheffield, Sheffield S3 7HF, UK.
§Present address: University of Lyon, Université Claude Bernard Lyon 1, CNRS, Institut Lumière Matière, 69622 Villeurbanne, France.

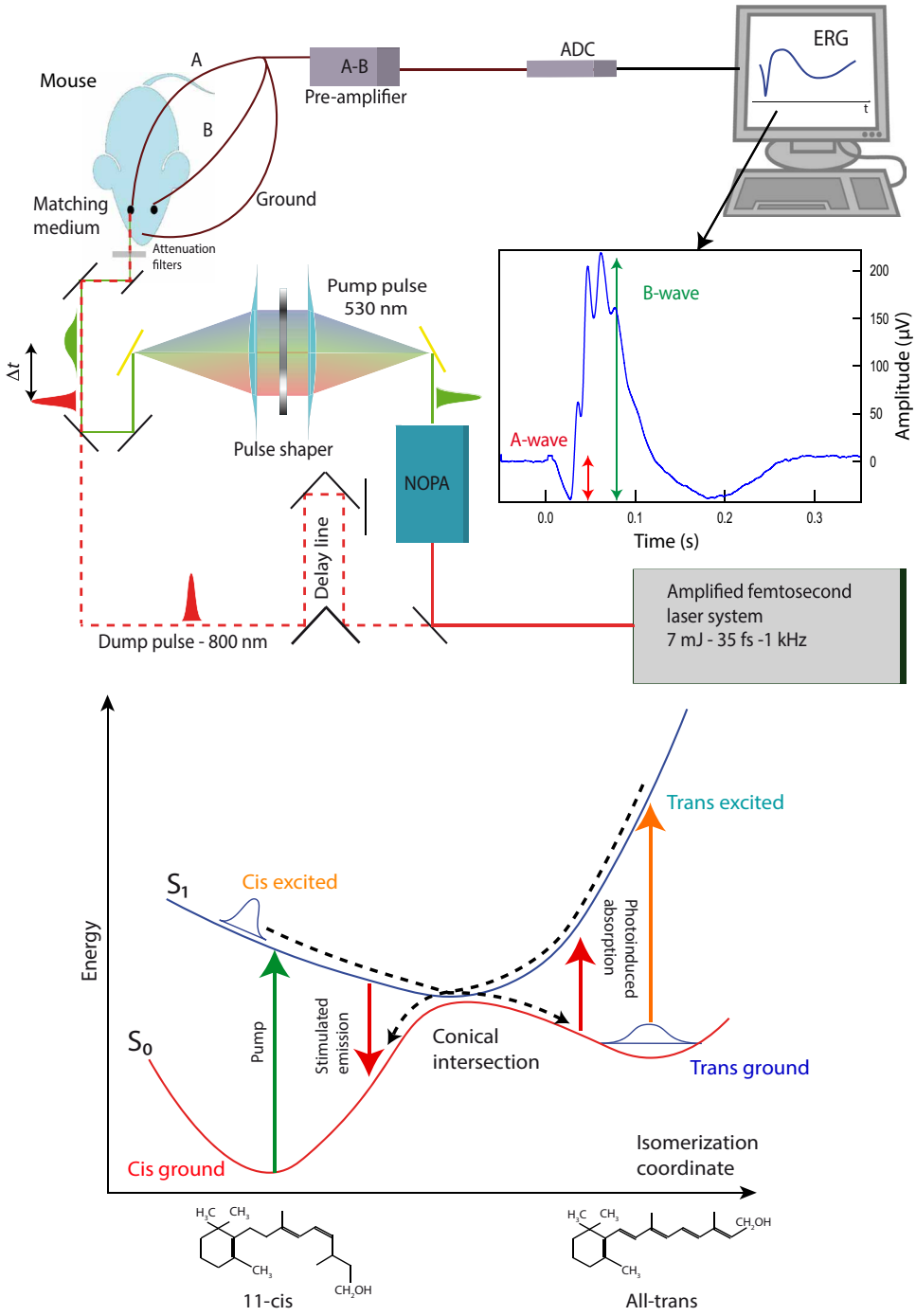

Fig. 1. Experimental setup and sketch of the energy surface of rhodopsin. (**Top**) Experimental setup: NOPA, noncollinear optical parametric amplifier; ADC, analog-to-digital converter. For the chirp dependence experiment, the near-infrared (NIR) pulse is blocked, and only the green laser pulse illuminates the eye of the mouse. For the two-color experiment, both pulses are used with the 535 nm compressed to near-zero chirp. (**Bottom**) Sketch of the energy surface of the rhodopsin as a function of the isomerization coordinate. The rhodopsin is promoted from the cis ground to the cis excited-state. The wave packet evolves through the conical intersection and can be either dumped by stimulated emission from the cis excited-state to the cis ground state or re-excited by absorption from the trans ground state to the trans excited-state.

the right eye of the mice every 2 s (i.e., a duty cycle of 0.002) to avoid cumulative effects and saturation of the visual transduction chain.

Within the first hundred milliseconds after illumination at 535 nm, the ERG trace shows two main features (Fig. 1): a small hyperpolarization (A-wave) directly followed by a more persistent depolarization (B-wave). The isomerization of the protonated Schiff base of retinal inside rhodopsin induces a biochemical cascade, which ends with the closing of ion channels in the rod membranes,

and is at the origin of the ERG A-wave. This hyperpolarization reduces the number of neurotransmitters released to the bipolar cells, leading to a depolarization that initiates the ERG B-wave.

As both pigments absorb light at 535 nm, all experiments were carried out on dark-adapted animals to favor scotopic vision, ensuring the silencing of cones and the recording of rod activity. The selective excitation of rods was shown by the analysis of rhodopsin knockout animals ($Rho^{del/del}$; fig. S1), in which medium cones did not generate any measurable signal below 3 nJ. This value was then used as the highest energy in the following experiment.

The 535-nm pulse, of 3-nJ energy, illuminated an area on the retina of 260 μm diameter, corresponding to an intensity of 1.1×10^8 W/cm^2. The diameter was measured at the position of the retina ex vivo (described in figs. S2 and S3). The near-infrared (NIR) pulse, even with energies up to 1 μJ, did not induce any substantial ERG signal associated with nonresonant two-photon absorption, which is in line with previously reported threshold values (fig. S4) (*19*). The ERG response from the mouse eyes did not degrade between the beginning and the end of the experimental procedure. Consequently, the laser illumination at these intensities induced neither chromophore damage nor pigment bleaching. The energy of the pump pulse is not limited by the risk of permanent retina alteration. To obtain the mean values and SEs indicated in Fig. 2, six datasets were acquired on three different mice. The *P* value associated to these measurements is 0.04.

As observed in Fig. 2, no difference in the ERG signal is observed when the NIR pulse precedes the visible pulse (negative delays), confirming that the 800-nm pulse has no effect on the rhodopsin molecules in their ground state. Conversely, when the 535-nm pulse first generates a vibrotorsional wave packet in the S_1 excited-state, the visual response is found to be modulated by the NIR component. More precisely, a first decrease of the A-wave occurs for a delay around 50 to 100 fs, as observed in Fig. 2 (A and B). This decrease is attributed to the dumping of the wave packet down to the 11-cis ground state by the 800-nm pulse, before it reaches the conical intersection, which reduces the 11-cis to all-trans photoisomerization in the retinal moiety.

Previous transient absorption measurements on solvated rhodopsin showed that the time required to cross the conical intersection is about 80 fs (*1*–*3*), which is in good agreement with our measurement in mice. A further decrease occurs at longer time delays, around 150 fs. At the conical intersection, the wave packet splits onto the different potential surfaces and a fraction of it propagates toward the all-trans ground state. We attribute the decrease around 150 fs to the repumping of molecules in the all-trans potential well to the all-trans excited-state, which leads to reverse isomerization by recrossing the conical intersection in the opposite direction (Fig. 2B). After a 200-fs delay, the molecule relaxes in the all-trans lowest vibronic state (*1*) and repumping by the 800-nm laser pulses is not possible anymore. Consequently, the retina response efficiency returns to its nominal value.

Quantum dynamics simulations were performed on the basis of the Hahn-Stock model Hamiltonian (*20*). This two-state two-mode diabatic model Hamiltonian has been parameterized to fit spectroscopic data. The two modes of this simplified model include the

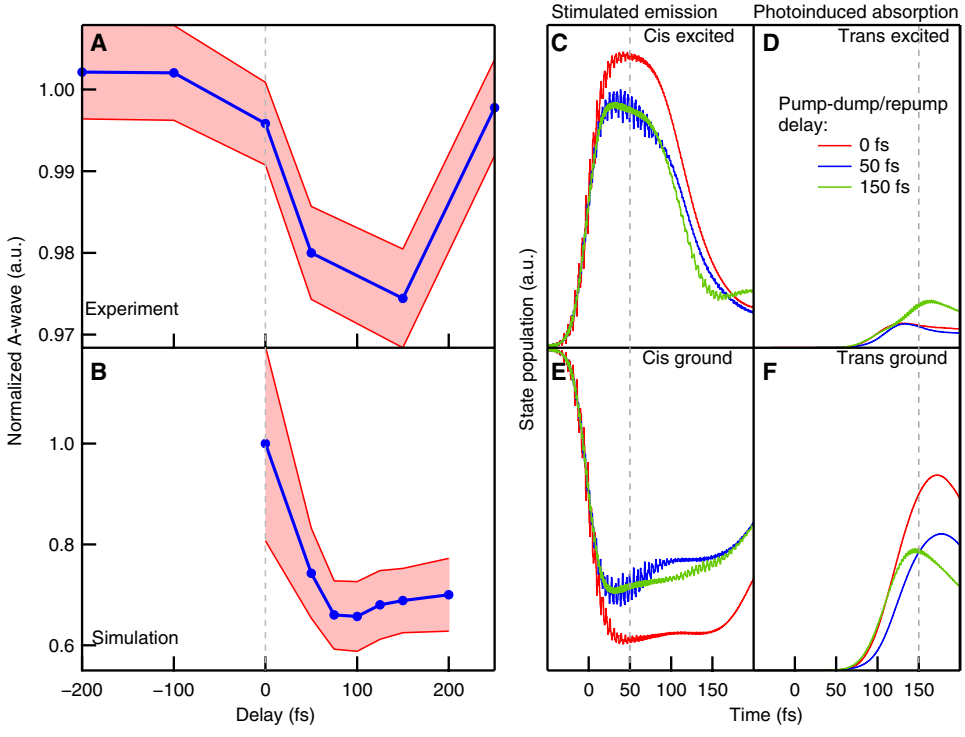

Fig. 2. Two-color pump-dump and pump-repump of retina response in living mice. (**A**) Measured normalized A-wave amplitude at different delays. Positive delays refer to green pulse preceding NIR pulse. The *P* value associated with this measurement is 0.04. The shaded area represents the SEM. (**B**) Quantum dynamics simulations of the two-color pump-dump/repump experiment. The shaded region represents the SD of the mean of the all-trans ground population calculated in the time span defined from the end of the dump pulse to 4 ps. (**C** to **F**) State populations as a function of delay. Populations of the cis excited (C), trans excited (D), cis ground (E), and trans ground (F) states as functions of time. a.u., arbitrary units.

reaction coordinate (delocalized torsion mode) as the tuning coordinate and a bond-length alternation of the backbone of the retinal chromophore as the coupling coordinate. The influence of the pulses on the nonadiabatic excited-state dynamics was simulated by including an explicit light-matter interaction term up to the dipole approximation. The details of the simulation setup are given in Table 1 and in Materials and Methods.

Two sets of simulations have been performed to simulate the two-color pump-dump experiments and the single chirped pulse experiments, the latter being explained below along with the corresponding experiment (for details of the simulation setup, see Materials and Methods). The results of the former are shown in Fig. 2 (B to F). Figure 2B depicts the running average of the product (trans ground state) population as a function of pump-dump delay normalized with respect to the one at zero delay. The photoproduct yield as a function of pump-dump delay follows the qualitative experimental trend shown in Fig. 2A with an initial decrease, a minimum of around 100 fs, and a subsequent increase at longer delay times. The characteristics of the underlying dynamics in these different regimes are illustrated for selected pump-dump delays of 0, 50, and 150 fs (Fig. 2, C to F). When the dump pulse coincides with the pump pulse (Fig. 2, C to F, red line), the dump does not have any significant effect on the overall dynamics since, right after photoexcitation, the wave packet remains close to the Franck-Condon zone. When the delay between the pump and the dump is 50 fs (Fig. 2, C and E, blue line), we observe a dump-induced resonant dumping of the wave packet from the first excited to the ground state occurring between 40 and 75 fs after excitation. As mentioned above, it is well known that the excited wave packet in rhodopsin takes approximately 80 fs (*1*–*3*) to reach the conical intersection. Therefore, the data are consistent with the first excited-state and the ground state being resonant with an 800-nm photon shortly before the wave packet crosses the conical intersection, thereby lowering the overall cis-trans isomerization yield. This dumping effect becomes even stronger for delays up to 100 fs, leading to a further decrease in photoisomerization product yield. After 100 fs, a significant portion of the wave packet moves through the conical intersection to the trans product state. Shortly after the crossing through the intersection, the wave packet can resonantly absorb an 800-nm photon to be re-excited to the S_1 state. This is illustrated by the 150-fs pump-dump delay simulations in Fig. 2 (C to F, green line). However, reabsorption is weaker than dumping for the pulse used, which helps regain the product yield to some extent.

It should be mentioned that in this model potential, the wave packet continues to remain highly delocalized. That is why both dumping and reabsorption are observed for time delays beyond 100 fs. The overall trend of the photoproduct yield, which correlates with the experimental A-wave amplitudes in the ERG signal, matches qualitatively. However, the regaining of the photoproduct formation obtained in the simulations for longer delays is lower compared to the experimental result, which might be due to the absence of environmental effects in the model. However, a recent multilayered multiconfiguration time-dependent Hartree (ML-MCTDH) simulation with the Hahn-Stock model shows that the addition of 23 Raman-active modes yields a significantly lower isomerization yield compared to the experimental value (*21*) and the photoproduct formation decreases further with the inclusion of more harmonic modes, showing that more appropriate bath models for use in the context of ML-MCTDH simulations have as yet to be developed for this system. To avoid possible artifacts due to the bath model, we prefer to present here the quantum dynamics results in the absence of additional bath modes.

Notice that reverse photoisomerization of the visual rhodopsin is usually assumed to be impossible in natural illumination conditions (*22*, *23*). This is definitely the case when the whole protein complex has relaxed in its final conformation (milliseconds) via the well-known photo, batho, lumi, and meta intermediates (*22*). However, on the femtosecond time scale, only the retinal moiety is addressed by the light excitation and the host protein structure remains unaffected. With the protein structure being intact, photoisomerization of retinal can be achieved in a transient manner, as it was recently confirmed experimentally in both bacteriorhodopsin

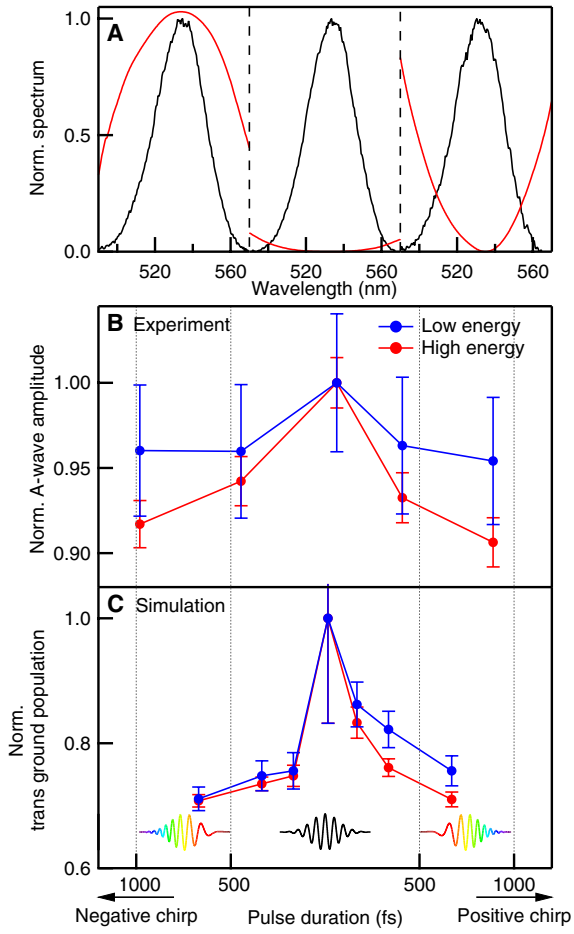

Fig. 3. Modulation of the perceived visual brightness by pulse shaping. (**A**) Measured spectrum (black) and phase (red) functions associated with the −2800, 300, and +3100 fs^2/rad pulses. (**B**) Measured normalized A-wave amplitude extracted from the ERG signal for five values of the pulse chirp (with $\varphi'' = -2800, -1400, 300, +1300,$ and +3100 fs^2/rad), modulating the ordering and delays of the frequencies in the pulse (linear chirp) and for two pulse energies (0.3 and 3 nJ). For the high-energy measurements, the *P* value calculated between the shortest pulse and the other conditions is always below 10^{-10}. For the low-energy measurements, the *P* value between the shortest pulse and the other conditions is always below 0.06, except for the point +408 fs ($P = 0.19$). Error bars represents the SEMs. (**C**) The average all-trans photoproduct yield as a function of chirp for higher (red) and lower (blue) intensities. The shaded region represents the SD of the mean of the all-trans ground population calculated in the time span defined from the end of the probe pulse to 4 ps.

Table 1. Details of the MCTDH simulation setup. Type of DVR, range (in a.u.), and number (*N*) of primitive grid points used for each vibrational coordinate. The number of single-particle functions (*n*) corresponding to the vibrational modes is given in the rightmost column. HO stands for harmonic oscillator–type DVR, and FFT stands for fast Fourier transform–type DVR. DOFs stands for degrees of freedom.

DOFs	DVR	Range	*N*	*n*
Backbone elongation	HO	[−8.0 to 8.0]	81	30
Torsion	FFT	[−π/2 to 3π/2]	256	30

and visual rhodopsin in solution using a pump-repump-probe technique (*8*, *9*).

The second approach that we adopted for the wave packet control of the rhodopsin in the retina is intrapulse femtosecond shaping, i.e., when the spectral components of the interacting light are ordered within the same laser pulse (*24*–*26*). This technique was already demonstrated in different retinal proteins, either in solutions [bovine rhodopsin, bacteriorhodopsin, and isorhodopsin (*5*, *7*, *27*, *28*)] or in patch clamp [channelrhodopsin (*14*)]. To this end, the choice of the 535-nm central wavelength is particularly judicious, as it allows the excitation of molecules from the ground states of both rhodopsin and photorhodopsin (*29*). Moreover 535 nm prevents initial excited-state absorption in rhodopsin of the higher-lying S_n states (*1*, *30*), which may compete with the desired reverse isomerization process.

The ERG signals are collected for different values of the spectral phase function φ(ω) within the laser pulses, which rigorously contain the same energy (i.e., the same number of photons). φ(ω) could be freely modulated in 640 spectral channels using a 4f-pulse shaper (Fig. 1). Each applied phase function was alternated with a reference flat phase function on the pulse shaper to prevent any long-term drift during the experiment.

Figure 3 shows the dependence of the eye sensitivity of living mice on the phase function $\varphi(\omega) = (\omega - \omega_0)^2\ \varphi''/2$ and, accordingly, the pulse duration (from 60 to 1000 fs FWHM). The A-wave amplitude, which is related to the number of isomerized rhodopsin, is clearly maximized for the flat phase, i.e., $\varphi'' = 300\ fs^2/rad$. Both negative and positive chirp functions reduce the eye response. This behavior is more pronounced for higher pulse energy (from 0.3 to 3 nJ), according to the nonlinear origin of the effect.

These results reveal that the rhodopsin-mediated retina response is sensitive to the spectral phase of light pulses as short as ~100 fs. In particular, the eye sensitivity is highest when the wavelengths are all ordered such that the pulse is the shortest. The associated higher instantaneous intensity does not produce a decrease of the retina response, as expected for nonlinear effects such as saturation or excited-state absorption in a higher-lying state S_n (*5*, *7*). On the contrary, short pulses yield the maximal photoisomerization. As already identified by the abovementioned two-color control experiment, the origin of this dependence lies in the dynamics along the retinal excited state S_1 and its conical intersection. The short 535-nm laser pulse produces a vibrotorsional wave packet, which crosses the conical intersection after 80 fs and splits to populate the desired photorhodopsin. After about 200 fs, the vibronic relaxation (*31*) in photorhodopsin leads to the desired all-trans isomer, which triggers the signaling chain until retina response. However, if the pulse duration is longer than ~80 fs, the reverse isomerization channel is opened, i.e., re-exciting the photorhodopsin and recrossing the conical intersection toward the ground state of the 11-cis. Consequently, the retina response is dependent on pulse duration so that both positive and negative chirped pulses lead to a decrease of this signal.

This interpretation is confirmed by the quantum dynamics simulations. Note that as the absorption band in photorhodopsin is Stokes-shifted by 30 nm as compared to rhodopsin, an asymmetry with the chirp sign could be anticipated. However, the calculations indicate that a bandwidth of at least 50 nm would be required to quantitatively observe this asymmetry under our experimental conditions, which is not the case in the present study.

The results of the quantum dynamics simulations for different chirped pulses are shown in Fig. 3C, which depicts the time-averaged trans-photoproduct yield (at 4 ps), as a function of chirp. Simulations at two different light pulse energies were performed. For the high-energy condition, we set the amplitude of the electric field three times larger than that of the lower-energy setting such that the energy ratio corresponds to 10, close to the experimental conditions. As it can be clearly seen from Fig. 3C, in agreement with the experimental observations (Fig. 3B), a chirped pulse always decreases the amount of photoproduct independent of the sign of the chirp with the maximum yield reached for the unchirped pulse. Larger chirps lead to even lower product yields, with higher intensities being more effective in decreasing photoproduct formation. These simulation results are in excellent qualitative agreement with corresponding experimental data (Fig. 3B). In addition, the simulations also indicate a slight asymmetry between positive and negative chirps, an effect that could not be resolved experimentally since a bandwidth of at least 50 nm would be required to observe such an asymmetry. However, note that while this simple two-dimensional model is capable of explaining all the major dynamical events occurring in the system on an ultrafast time scale, a fully quantitative comparison with experiments is probably beyond what can be expected from such a simplified model.

In conclusion, we have demonstrated that the physiological response of the retina in living mice can be modulated acting on the ultrafast dynamics of rhodopsin, using two complementary photodynamical schemes: two-color pump-dump/repump and femtosecond intrapulse shaping. The interaction mechanism, which emerges from these measurements and the supporting numerical simulation, relies on steering the dynamics of a vibronic wave packet evolving on the S_1 excited-state in rhodopsin either by transferring it to the cis ground state by stimulated emission before it reaches the conical intersection leading to the isomerization or by reversing the isomerization by repumping the wave packet back to the cis configuration before it settles in the well of the trans ground state. The synergetic combination of the two interactions leads to a net decrease of the signals fired from the retina of the animal, with up to a 7% statistical difference with respect to the control experiments. The fact that control could be achieved at physiological intensities opens perspectives for applications involving information encrypted in the spectral phase of light pulses.

MATERIALS AND METHODS

Chirp experiment

An amplified Ti:sapphire laser system (Astrella by Coherent Inc.) delivering a 35-fs pulse at 800-nm central wavelength with a 1-kHz repetition rate pumps a noncollinear optical parametric amplifier (NOPA; TOPAS-White by Light Conversion). The NOPA output (50-fs, 535-nm central wavelength $\Delta\lambda$ = 30 nm FWHM) is temporally shaped by a spatial light modulator (SLM-S640 by Jenoptik) in a 4f-line. A fast silicon photodiode combined to a gated integrator measures the energy of each pulse, and a combination of a half–wave plate and a polarizer mounted on a computer-controlled motorized rotational stage allows maintaining a constant average pulse energy at varying SLM settings. For each setting, the chirp is measured by taking an Second Harmonic Generation Frequency-Resolved Optical Gating (SHG FROG) (APE PulseCheck). A fast electronic shutter (Newport model 76992) allows five pulses to illuminate one eye of the mouse under study with a 2-s duty cycle.

Double-pulse experiment

The output from the Ti:sapphire amplifier is split into two pulse trains: one pumps the NOPA, and its 50-fs, 535-nm output is kept unchirped (pump pulse), attenuated to 3 nJ, and coupled onto the mouse eye. The second (dump/repump pulse) at 800 nm and 1 μJ is compressed to 50 fs FWHM by multiple reflections on chirped mirrors and is subsequently recombined in a collinear way with the pump pulse through a beam splitter. The pulses are coupled onto the mouse eye in the same fashion as in the chirp experiment; the fast shutter allows five pump-dump pulse pairs to illuminate one eye (illumination event). A computer-controlled, motorized linear stage (PI model M-505.4DG) on the optical path of the dump pulse sets the temporal delay between the two pulses.

Detection system

A tinned copper ring (3 mm diameter) connected to an electrical wire is centered and put in contact with each of the eyes of the animal. An additional wire in the mouse mouth provides electrical grounding. A triggering software controls both the illumination event and the ERG acquisition: The differential bio-electric signal from the two eyes is amplified and band-pass–filtered with a preamplifier (SR560 by Stanford Research System Inc.) working on battery power. The anesthetized mouse and the preamplifier are enclosed in a custom-made Faraday cage to reduce the 50-Hz noise pickup. The analog signal is digitized by an analog-to-digital converter (PCI-6220 by National Instruments) with a sampling frequency of 25 kHz connected to a computer and controlled by a dedicated acquisition software. During a data acquisition run, the ERG signal is typically sampled a few milliseconds before and after a single illumination event.

Analysis

Linear regression is performed on the first 1000 sampled ERG data points collected before each illumination event to determine the differential baseline. The signal is subsequently Fourier-filtered (low pass at 50 Hz, FIR order 1501). In this way, the amplitudes of the A- and B-waves are directly measured from the minimum and maximum values of the ERG. For each statistical datasets, outliers are removed following Chauvenet's criterion (*32*).

For the chirp experiment, data are normalized to the maximum values corresponding to the FT (Fourier-transformed) pulses. The results shown for the 3-nJ case is the average over seven mice (11 datasets of 45 min), while the experiment at 0.3 nJ is the average over the results on four mice (7 datasets of 45 min). The *P* values presented in Fig. 3 are computed with the one-sample *t* test. The error bars in all experimental plots correspond to SEMs.

For the pump-dump experiment, data are normalized to a reference taken as the average over the negative pump-dump delays (infrared pulse preceding the green pump). The results shown consist of an average of six datasets conducted on three mice. The *P* value presented in Fig. 2 is achieved by a one-sided analysis of variance (ANOVA).

Animals

Mice were housed and handled in accordance with the guidelines and regulations of the institution and of the state of Geneva (authorization number 29604). C57BL/6 male mice were purchased from Charles River Laboratories. *Opn1mw*^{del} and *Rho*^{del} animals were generated and housed at the University of Geneva.

Animal procedure

Mice were dark-adapted for 2 hours before experiments. They were anesthetized with an intraperitoneal injection of ketamine (90 mg/kg) and xylazine (10 mg/kg) solution under dim red light (PF712 Dr FISCHER). Forty-five minutes after the primary injection and every 40 min, a solution of ketamine (15 mg/kg) and xylazine (3 mg/kg) was injected to maintain anesthesia, for a total duration of 2 hours and 30 min of anesthesia. The temperature of the mice was maintained using a hand warmer and a cover. After the initial anesthesia, one drop of mydriatic (Mydriaticum Dispersa, 5 mg/ml; Omnivision) was deposited on each eye. Ring electrodes were then applied on both eyes. To improve the conductance of the signal between the eyes and the electrodes and to maintain moisture, drops of 2% hydroxypropyl-methylcellulose (Methocel 2%; Omnivision) were regularly casted on the reference eye. A small tube filled with methylcellulose was apposed to the stimulated eye, with a flat glass window on the laser side of the tube. This arrangement prevented focusing of the beam on the retina since the methylcellulose solution has the same refraction index as the cornea and the entrance pupil was flat.

Generation of knockout animals

Knockout animals were generated using CRISPR-Cas9. Pronuclei were injected with a mix of Cas9 mRNA and specific guide RNAs targeting the coding sequence of the mouse *Rho* or the *Opn1mw* opsin genes.

The *Opn1mw*^{del} allele (*Opn1mw*^{em1Irod}) has a 31–base pair (bp) deletion and a 2-bp insertion (AA) in the coding exon 2 of the *Opn1mw* gene (deletion of nucleotides 361 to 391). This mutation generates a frameshift and the potential production a protein divergent from the wild-type sequence from amino acid 120 (the wild-type protein is 359 amino acids long) and leads to a STOP codon at amino acid 149.

The *Rho*^{del} allele (*Rho*^{em1Irod}) has a 1-bp insertion in the *Rho* mouse gene (insertion of an A between nucleotides 216 and 217). This mutation generates a frameshift mutant with a protein sequence divergent from the wild-type sequence from amino acid 72 (the wild-type protein is 349 amino acids long) and leads to a STOP codon at amino acid 82.

Quantum dynamics simulations

Non-adiabatic quantum dynamics simulations were performed with the MCTDH wave packet propagation scheme (*33*) implemented

within the Quantics package (*34*). The time-dependent Schrödinger equation was solved for the (time-dependent) Hamiltonian including the light-matter interaction term up to the dipole approximation. The model Hamiltonian includes two electronic states and two vibrational modes within a linear vibronic coupling scheme (*20*). The initial wave packet was prepared in the form of a direct product discrete value representation (DVR) grid, the details of which are provided in the table below.

As the propagation of the wave packet has been done in the diabatic representation, the population of the different electronic states are also calculated in the same representation in a straightforward way. The population of the diabatic state $|a\rangle$ at time t, denoted by $P_a(t)$, is given by

$$P_a(t) = \langle \psi(\mathbf{R}, t) \,|\, a \rangle \langle a \,|\, \psi(\mathbf{R}, t) \rangle$$

where $\Psi(\mathbf{R},t)$ is the total molecular wave function of the system. The integration is performed over the whole grid of nuclear coordinates. However, we have differentiated cis and trans forms in terms of the range of integration along the torsional-type coordinate; namely, cis populations are obtained when the torsional coordinate is integrated in the range $[-\pi/2$ to $\pi/2]$ and the trans populations are obtained for the range $[\pi/2$ to $3\pi/2]$. The fast FT (FFT)–type DVR takes care of the full periodicity of the torsional potential.

The light-induced dynamics of course depends on the transition-dipole moment between the two electronic states. Here, we have adopted the commonly used Condon approximation; in other words, we have assumed that the transition-dipole moment is constant for the duration of the pulse, and the constant value is arbitrarily set to 1 atomic unit (a.u.). Moreover, the dynamics has been conducted in the diabatic representation, in which the transition-dipole moment can be assumed to be a smooth function of coordinates, even close to the conical intersection. The numerical light pulses used in the simulations have been assumed to have a Gaussian envelope. For the pump-dump experiment, the pump is parametrized to have a central wavelength of 500 nm and a spectral bandwidth of 10 nm. The use of different pulse parameters in the simulation compared to the experimental ones (500 nm versus 535 nm) is necessitated by the fact that the absorption spectrum of the two-dimensional model potential is not broad enough to absorb a 535-nm pulse efficiently. The dump pulse, on the other hand, has a central wavelength of 800 nm with a spectral bandwidth of 20 nm. For the chirped pulses, we have used a central wavelength of 530 nm and a spectral bandwidth of 100 nm. Chirps have been introduced within the range of $[-1000$ to $1000]$ rad/fs^2, which effectively provides similar pulse durations as used in the experiments. For the simulation of the pump-dump experiments, the amplitude of the NIR (dump) pulse has been made three times that of the pump pulse to enhance its influence for the sake of clear detection. For the second set of experiments using chirped pulses, we have performed two sets of simulations differing in the amplitudes of the chirped pulses used. The lower-amplitude ones have a maximum amplitude of 0.005 a.u., while the higher ones are three times higher, giving rise to approximately the experimental condition of increasing the energy by one order of magnitude.

To use the entire frequency range of the chirped pulses, we have prepared the system in the first excited-state and the pulse is switched on from the beginning of the simulation. As a function of chirp, different frequency components can interact with the system at different times of the dynamics, opening up the possibility to probe different temporal events.

SUPPLEMENTARY MATERIALS

Supplementary material for this article is available at http://advances.sciencemag.org/cgi/content/full/7/18/eabe1911/DC1

REFERENCES AND NOTES

1. D. Polli, P. Altoè, O. Weingart, K. M. Spillane, C. Manzoni, D. Brida, G. Tomasello, G. Orlandi, P. Kukura, R. A. Mathies, M. Garavelli, G. Cerullo, Conical intersection dynamics of the primary photoisomerization event in vision. *Nature* **467**, 440–443 (2010).
2. R. W. Schoenlein, L. A. Peteanu, R. A. Mathies, C. V. Shank, The first step in vision: Femtosecond isomerization of rhodopsin. *Science* **254**, 412–415 (1991).
3. C. Schnedermann, M. Liebel, P. Kukura, Mode-specificity of vibrationally coherent internal conversion in rhodopsin during the primary visual event. *J. Am. Chem. Soc.* **137**, 2886–2891 (2015).
4. C. Brif, R. Chakrabarti, H. Rabitz, Control of quantum phenomena: Past, present and future. *New J. Phys.* **12**, 075008 (2010).
5. V. I. Prokhorenko, A. Halpin, P. J. M. Johnson, R. J. D. Miller, L. S. Brown, Coherent control of the isomerization of retinal in bacteriorhodopsin in the high intensity regime. *J. Chem. Phys.* **134**, 085105 (2011).
6. C. J. Bardeen, Q. Wang, C. V. Shank, Femtosecond chirped pulse excitation of vibrational wave packets in LD690 and bacteriorhodopsin. *J. Phys. Chem. A* **102**, 2759–2766 (1998).
7. A. C. Florean, D. Cardoza, J. L. White, J. K. Lanyi, R. J. Sension, P. H. Bucksbaum, Control of retinal isomerization in bacteriorhodopsin in the high-intensity regime. *Proc. Natl. Acad. Sci. U.S.A.* **106**, 10896–10900 (2009).
8. O. Smitienko, V. Nadtochenko, T. Feldman, M. Balatskaya, I. Shelaev, F. Gostev, O. Sarkisov, M. Ostrovsky, Femtosecond laser spectroscopy of the rhodopsin photochromic reaction: A concept for ultrafast optical molecular switch creation (ultrafast reversible photoreaction of rhodopsin). *Molecules* **19**, 18351–18366 (2014).
9. T. B. Feldman, O. A. Smitienko, I. V. Shelaev, F. E. Gostev, O. V. Nekrasova, D. A. Dolgikh, V. A. Nadtochenko, M. P. Kirpichnikov, M. A. Ostrovsky, Femtosecond spectroscopic study of photochromic reactions of bacteriorhodopsin and visual rhodopsin. *J. Photochem. Photobiol. B Biol.* **164**, 296–305 (2016).
10. G. Vogt, P. Nuernberger, T. Brixner, G. Gerber, Femtosecond pump–shaped-dump quantum control of retinal isomerization in bacteriorhodopsin. *Chem. Phys. Lett.* **433**, 211–215 (2006).
11. M. Shapiro, P. Brumer, *Quantum Control of Molecular Processes* (John Wiley & Sons, 2012).
12. Y. Silberberg, Quantum coherent control for nonlinear spectroscopy and microscopy. *Annu. Rev. Phys. Chem.* **60**, 277–292 (2009).
13. D. J. Tannor, R. Kosloff, S. A. Rice, Coherent pulse sequence induced control of selectivity of reactions: Exact quantum mechanical calculations. *J. Chem. Phys.* **85**, 5805–5820 (1986).
14. K. Paul, P. Sengupta, E. D. Ark, H. Tu, Y. Zhao, S. A. Boppart, Coherent control of an opsin in living brain tissue. *Nat. Phys.* **13**, 1111–1116 (2017).
15. G. S. Engel, T. R. Calhoun, E. L. Read, T.-K. Ahn, T. Mančal, Y.-C. Cheng, R. E. Blankenship, G. R. Fleming, Evidence for wavelike energy transfer through quantum coherence in photosynthetic systems. *Nature* **446**, 782–786 (2007).
16. A. Ishizaki, G. R. Fleming, Theoretical examination of quantum coherence in a photosynthetic system at physiological temperature. *Proc. Natl. Acad. Sci. U.S.A.* **106**, 17255–17260 (2009).
17. J. Cao, R. J. Cogdell, D. F. Coker, H.-G. Duan, J. Hauer, U. Kleinekathöfer, T. L. C. Jansen, T. Mančal, R. J. D. Miller, J. P. Ogilvie, V. I. Prokhorenko, T. Renger, H.-S. Tan, R. Tempelaar, M. Thorwart, E. Thyrhaug, S. Westenhoff, D. Zigmantas, Quantum biology revisited. *Sci. Adv.* **6**, eaaz4888 (2020).
18. I. Perlman, The electroretinogram: ERG. *Webvision: The Organization of the Retina and Visual System* (2007); https://webvision.med.utah.edu/book/electrophysiology/the-electroretinogram-erg/.
19. G. Palczewska, F. Vinberg, P. Stremplewski, M. P. Bircher, D. Salom, K. Komar, J. Zhang, M. Cascella, M. Wojtkowski, V. J. Kefalov, K. Palczewski, Human infrared vision is triggered by two-photon chromophore isomerization. *Proc. Natl. Acad. Sci. U.S.A.* **111**, E5445–E5454 (2014).
20. S. Hahn, G. Stock, Femtosecond secondary emission arising from the nonadiabatic photoisomerization in rhodopsin. *Chem. Phys.* **259**, 297–312 (2000).
21. M. Sala, D. Egorova, Quantum dynamics of multi-dimensional rhodopsin photoisomerization models: Approximate versus accurate treatment of the secondary modes. *Chem. Phys.* **515**, 164–176 (2018).
22. O. P. Ernst, D. T. Lodowski, M. Elstner, P. Hegemann, L. S. Brown, H. Kandori, Microbial and animal rhodopsins: Structures, functions, and molecular mechanisms. *Chem. Rev.* **114**, 126–163 (2014).

23. K. Sato, T. Yamashita, H. Ohuchi, A. Takeuchi, H. Gotoh, K. Ono, M. Mizuno, Y. Mizutani, S. Tomonari, K. Sakai, Y. Imamoto, A. Wada, Y. Shichida, Opn5L1 is a retinal receptor that behaves as a reverse and self-regenerating photoreceptor. *Nat. Commun.* **9**, 1255 (2018).
24. T. Brixner, N. H. Damrauer, P. Niklaus, G. Gerber, Photoselective adaptive femtosecond quantum control in the liquid phase. *Nature* **414**, 57–60 (2001).
25. R. S. Judson, H. Rabitz, Teaching lasers to control molecules. *Phys. Rev. Lett.* **68**, 1500–1503 (1992).
26. A. Goun, D. I. Bondar, A. O. Er, Z. Quine, H. A. Rabitz, Photonic reagents for concentration measurement of flu-orescent proteins with overlapping spectra. *Sci. Rep.* **6**, 25827 (2016).
27. V. I. Prokhorenko, A. M. Nagy, S. A. Waschuk, L. S. Brown, R. R. Birge, R. J. D. Miller, Coherent control of retinal isomerization in bacteriorhodopsin. *Science* **313**, 1257–1261 (2006).
28. M. Liebel, P. Kukura, Lack of evidence for phase-only control of retinal photoisomerization in the strict one-photon limit. *Nat. Chem.* **9**, 45–49 (2017).
29. H. Kandori, Y. Shichida, T. Yoshizawa, Photoisomerization in rhodopsin. *Biochemistry (Moscow)* **66**, 1197–1209 (2001).
30. I. Rivalta, A. Nenov, O. Weingart, G. Cerullo, M. Garavelli, S. Mukamel, Modelling time-resolved two-dimensional electronic spectroscopy of the primary photoisomerization event in rhodopsin. *J. Phys. Chem. B* **118**, 8396–8405 (2014).
31. P. J. M. Johnson, A. Halpin, T. Morizumi, V. I. Prokhorenko, O. P. Ernst, R. J. D. Miller, Local vibrational coherences drive the primary photochemistry of vision. *Nat. Chem.* **7**, 980–986 (2015).
32. L. Lin, P. D. Sherman, Cleaning data the Chauvenet way, in *The Proceedings of the SouthEast SAS Users Group, SESUG Proceedings, Paper SA11* (SESUG, 2007), pp. 1–11.
33. H.-D. Meyer, U. Manthe, L. S. Cederbaum, The multi-configurational time-dependent Hartree approach. *Chem. Phys. Lett.* **165**, 73–78 (1990).
34. G. A. Worth, Quantics: A general purpose package for quantum molecular dynamics simulations. *Comput. Phys. Commun.* **248**, 107040 (2020).

Acknowledgments: We acknowledge M. Moret, V. P. Jungo, and J.-M. Matter for invaluable help regarding the technical support. **Funding:** This work was supported by the SNSF (Swiss National Science Foundation) under Sinergia grant number CRSII5_170981 and the NCCR-MUST (Molecular Ultrafast Science and Technology). **Author contributions:** G.G., C.S., A.C., S.H., and L.B. mounted the setup and created the software for acquisition and analysis. G.G. and Q.D. acquired and analyzed the data with help from F.C. and M.M. Q.D. and I.R. handled and supervised the animal aspects. S.B. and U.R. set up, run, and analyzed the numerical simulations. P.L.H., I.R., and J.-P.W. administrated the project and acquired the funding. U.R., I.R., and J.-P.W. conceived the experiment. G.G., Q.D., S.B., L.B., U.R., I.R., and J.-P.W. wrote the paper. All authors approved the manuscript. **Competing interests:** The authors declare that they have no competing interests. **Data and materials availability:** All data needed to evaluate the conclusions in the paper are present in the paper and/or the Supplementary Materials. Additional data related to this paper may be requested from the authors.

Submitted 5 August 2020
Accepted 9 March 2021
Published 28 April 2021
10.1126/sciadv.abe1911

Citation: G. Gaulier, Q. Dietschi, S. Bhattacharyya, C. Schmidt, M. Montagnese, A. Chauvet, S. Hermelin, F. Chiodini, L. Bonacina, P. L. Herrera, U. Rothlisberger, I. Rodriguez, J.-P. Wolf, Ultrafast pulse shaping modulates perceived visual brightness in living animals. *Sci. Adv.* **7**, eabe1911 (2021).